Journal of Alloys and Compounds 509 (2011) 8870–8879

Contents lists available at ScienceDirect

Journal of Alloys and Compounds

journal homepage: www.elsevier.com/locate/jallcom

The influence of solution treatment temperature on microstructure and corrosion behavior of high temperature ageing in 25% Cr duplex stainless steel

Y.H. Yang[a,b], B. Yan[a,b,*], J. Wang[a,b], J.L. Yin[a,b]

[a] School of Materials Science and Engineering, Tongji University, Shanghai 200092, China
[b] Shanghai Key Lab of D&A for Metal-Functional Materials, Shanghai 200092, China

ARTICLE INFO

Article history:
Received 19 September 2010
Received in revised form 8 June 2011
Accepted 23 June 2011
Available online 30 June 2011

Keywords:
Solution treatment temperature
Duplex stainless steels
Ageing
σ-Phase

ABSTRACT

In 25% Cr duplex stainless steels, the effect of prior-solution treatment temperature (STT) on the microstructure and corrosion behavior with ageing at 750 °C and 850 °C was investigated. The results revealed that the precipitation rate of σ-phase was fast in the early stage of ageing for 80 min, and then got slower with ageing time up to 330 min. The σ-phase formation was effectively suppressed by raising STT from 1060 °C to 1230 °C especially for ageing at 750 °C. Consequently, the corrosion rate of specimen was dependent on the amount of σ-phase precipitation, and was lowered due to higher STT, and more σ-phase precipitation can lead to the transition from metastable to stable pitting with ageing at 750 °C up to 330 min. Pitting occurred easily around coarse σ precipitates and caused selective dissolution in ferrite. The longer ageing time increased intergranular corrosion (IGC) susceptibility, whereas higher STT contributed to better resistance to IGC.

1. Introduction

Duplex stainless steels (DSS) are composed of approximately equal volumetric fractions of ferrite and austenite, displaying superior mechanical properties and corrosion resistance in an ample range of applications, and are thus extensively used in several fields such as chemical processing, marine and desalination industries [1–4]. In most cases, DSS are chosen based on their strength and passivation state in various environments. Nevertheless, if DSS are exposed to a certain range of high temperature for a longer time, the balance of alloying elements can be disturbed by precipitation of various secondary phases. The most common precipitates are secondary austenite (γ_2), nitrides, $M_{23}C_6$ carbide and Fe–Cr–Mo intermetallic phases such as σ-phase and χ-phase [5,6]. Their presence can cause time-dependent degradation of the material particularly in its corrosion properties. Among these secondary precipitates, σ-phase with fast formation kinetics can cause a dramatic deterioration in the toughness and corrosion resistance of DSS.

The σ-phase can be observed with ageing at the temperature range of 475–1000 °C. Furthermore, ageing at the temperature range of 650–975 °C is considered most dangerous due to more σ-phase precipitation in DSS [7,8]. In addition, the time–temperature–transformation diagram also exhibited that the nose of σ-phase transformation was located at 800 °C in cast 22 wt.% Cr DSS [9], indicating that ageing temperature around 800 °C can cause initial σ-phase precipitation. Therefore, it is important to investigate σ-phase precipitation and corresponding corrosion behavior in this temperature range because high temperature processing is necessary in production. Since the currently-used DSS contain very low carbon, the intergranular corrosion (IGC) is mainly caused by submicroscopic σ-phase precipitates, other than carbide precipitation such as $Cr_{23}C_6$ [10]. Double loop electrochemical potentiokinetic reactivation (DL-EPR) test is generally used to evaluate the intergranular corrosion, because it can provide a quantitative value of the degree of sensitization instead of mere qualitative appreciation like metallographic etchings [11].

It is taken for granted that pitting corrosion resistance depends basically on the content of Cr, Mo and N. The Cr- and Mo-rich σ-phase preferentially nucleates at δ/γ interface or within δ grains, leading to the Mo- and Cr-depleted region around it, thus favoring the pitting corrosion. Pitting is also the precursor to stress corrosion cracking because it provides a combination of local aggressive solution chemistry and stress-concentrating feature. On the other hand, solution treatment is an effective way to maintain the high resistance to localised corrosion, by which the alloying elements can be in solid solution and homogeneously distributed in metal in order to attain passivation effect. However, different solution treatment temperatures (STT) can result in different changes in volumetric equilibrium fraction of δ and γ phases in DSS, and Cr and Mo content in the two phases is altered accordingly. Therefore, it

* Corresponding author at: School of Materials Science and Engineering, Tongji University, Shanghai 200092, China. Tel.: +86 21 659 811 78; fax: +86 21 659 853 85.
E-mail addresses: yyhyanr@sina.com (Y.H. Yang), yanbiao_tj@163.com (B. Yan).

0925-8388/$ – see front matter © 2011 Elsevier B.V. All rights reserved.
doi:10.1016/j.jallcom.2011.06.099

is important to delay the σ-phase formation by taking appropriate heat treatment measures. Lai et al. [12] found that the STT affected the amount and morphology of δ-ferrite, and the volume fraction of larger-grain-size ferrite increased when the STT was elevated. Recently, some researches have reported that raising the STT from 1050 to 1250 °C delays the σ-phase formation and favors the precipitation of intragranular secondary austenite (γ_2) in weld metal of 2205 duplex stainless steels [13]. Meanwhile, the retardation of σ-phase precipitation has been reported as the STT increased from 1080 °C to1200 °C during continuous cooling procedure [14]. However, there is little research available concerning the relevance of microstructural evolution of high temperature ageing to corrosion resistance behavior due to increased STT.

Technically, we can take some measures to suppress the σ-phase precipitation. The basic way is to reduce the Cr and Mo contents in the smelting process, but this will lower the resistance to pitting corrosion. Meanwhile, the PREN number, which was commonly used to rank stainless steels with respect to their resistance to pitting corrosion according to the following relation [15]: PREN = wt.%Cr + 3.3 wt.%Mo + 16 wt.%N, is lowered simultaneously. Instead, it is a relatively simple way by taking appropriate heat treatment route to delay the σ-phase precipitation to improve the performance of DSS. As a result, in high temperature ageing at 750 °C and 850 °C, the effect of prior-STT on the σ-phase formation and corrosion behavior was investigated intensively.

2. Experimental

The material used in this study was a commercial 2507 type steel bar (60 mm in diameter) and the chemical composition of the alloy is listed in Table 1. The solution treatments were performed at 1060 °C and 1230 °C respectively and held for 30 min, followed by water quenching. Then specimens were examined by optical microscopy (OM). Phase volume fractions of δ-ferrite and γ-austenite were calculated using the method of manual point count according to ASTME 562 as follows: a magnification of the optical micrograph was ×200 and a grid size (number of points, PN) was 10 × 10. Any point that fell on the phase studied was counted as one, otherwise zero. Exceptionally, that fell on the boundary was counted as a half [16].

In order to investigate the effect of the STT on the microstructure and corrosion behaviors, the ageing treatment for solution treated specimens was carried out at 750 °C and 850 °C with time varying from 30 min to 330 min, respectively. The mechanically polished samples were electrolytically etched in 40 wt.% KOH solution at 6 V for 15 s before examined by scanning electron microscopy (SEM). In addition, the presence of different phases in the specimens was determined by X-ray diffraction analysis (XRD) and the phase composition of the alloy was analysed by electron dispersive X-ray spectroscopy (EDX) attached to SEM. In order to understand how ageing time affects the decomposition process of δ-ferrite, quantitative metallographic measurement of δ-ferrite phase and σ-phase was also carried out by using manual point counting. The magnification of scanning electron micrograph was ×2000 and a grid size was 20 × 20, requested by ASTME 562 that phase volume fractions below 2% like σ-phase in the case should be of 20 × 20 instead of 10 × 10 [16].

Prior to potentiodynamic anodic polarization and DL-EPR tests, the sample surface was wet-polished successively from 600- to 2000-gradation abrasive sandpaper, followed by sonication in deionised water for 5 min. The samples were further polished using an emulsion of 0.05 μm SiC particles under high frequency vibration conditions, to obtain a mirror-like surface. The corrosion resistance evaluation was determined using potentiodynamic anodic polarization test in a deaerated 3.5 wt.% NaCl solution at 30 °C, from −600 mV SCE to about 1000 mV SCE, where the transpassivity occurred indicated by the results of current density. The specimens of 10 mm×10 mm plates acting as working electrodes were embedded in epoxy resin, with platinum foil as the counter electrode and saturated calomel electrode (SCE) as reference electrode. SEM was used again to observe corrosion morphology on the specimens after the potentiodynamic measurements. The susceptibility to intergranular corrosion was evaluated by DL-EPR test, which was conducted in the solution of 1 M H_2SO_4 + 0.5 M NaCl + 0.01 M KSCN at 30 ± 1 °C with a scan rate of 1 mV/s, where the role of KSCN and NaCl is to break the passive film during the reactivation cycle of the test [17]. The three-electrode cell was the same as used in potentiodynamic anodic polarization measurement. The working electrode of the DSS samples was embedded in epoxy resin, polished to diamond finish (1.5 μm), rinsed in acetone and dried in the hot air before each experiment. The potential was scanned in the anodic direction from the corrosion potential (E_{corr}) to the point of 0.250 V in the middle of the passive region and the scanning direction was then reversed with the potential reduced back to the cathodic region. Two loops were generated in this way: an anodic loop and a reactivation loop. The maximum current density in the anodic scan loop (I_a) and in the reversed scan loop (I_r) were both measured. The degree of sensitization (R_a) was compared by the value of $(I_r/I_a) \times 100$.

3. Results and discussion

3.1. Microstructural and morphological analysis

Fig. 1 shows the optical microstructure of the specimens after solution treatment at 1060 °C and 1230 °C, respectively. Darker phases represent δ-ferrite and brighter phases are γ-austenite. The island-like γ-phase was surrounded with the continuous matrix of δ-phase. And the results of the manual point counting showed that the volume fraction of ferrite with solution treatment at 1060 °C and 1230 °C was 48.9% and 52.4% respectively, indicating a better balance of both phases. In addition, the volume fraction of ferrite was increased with higher STT.

Fig. 2 shows the microstructures of DSS aged at 750 °C and 850 °C after solution treatment at 1060 °C and 1230 °C, respectively. As can be seen, the duplex structure remains and the light grey region represents δ-ferrite, the dark grey region represents γ-austenite, while the coarse white precipitates identified as σ-phase are predominantly distributed at δ/γ interface and within δ-ferrite matrix. Among them, Fig. 2a and b present the microstructures obtained from the specimens aged at 750 °C for 60 min after solution treatment at 1060 °C and 1230 °C for 30 min, respectively. We noticed that the transformation of $\delta \rightarrow \sigma + \gamma_2$ occurs easily in DSS with δ-ferrite enriched σ-phase forming elements (Cr, Mo) during high temperature ageing. Hence, in the early stage of δ-ferrite

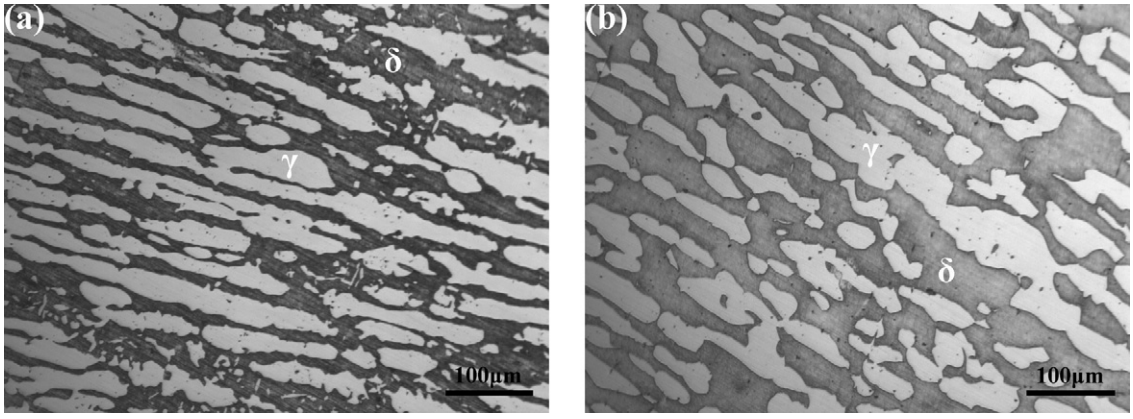

Fig. 1. Optical micrographs of the specimens: solution treatment at (a) 1060 °C and (b) 1230 °C.

Table 1
Chemical composition (wt.%) of the alloy used.

C	Mn	Si	S	P	Ni	Cr	Mo	Cu	N	Fe
0.019	0.56	0.40	0.017	0.032	6.28	24.67	3.20	0.28	0.27	Bal.

transformation, small σ particles predominantly precipitate at δ/γ interface. By contrast, increasing STT from 1060 °C to 1230 °C led to less amount of σ-phase precipitation at δ/γ interface. Both the size and amount of σ-phase increased rapidly by prolonging the ageing time at 750 °C to 80 min, as it became coarser and developed into lamellar particles within δ-ferrite grains. In comparison with STT at 1060 °C (Fig. 2c), 1230 °C (Fig. 2d) contributed to smaller σ-phase particles, which were dispersed within ferrite grains and at δ/γ interface. Fig. 2e and f present SEM micrographs of the samples aged at 850 °C for 60 min after STT at 1060 °C and 1230 °C for 30 min, respectively. At higher ageing temperature (850 °C), coarser σ particles appeared at δ/γ interfaces and a few were distributed within the ferrite grains, suggesting an enhanced role of solute elements (Cr, Mo) within the δ-ferrite matrix. With further ageing at 850 °C for 80 min, σ-phase particles were ever-coarsening within δ-ferrite grains and at δ/γ interface. Meanwhile, it was observed that increasing STT from 1060 °C (Fig. 2g) to 1230 °C (Fig. 2h) led to smaller σ-phase formation.

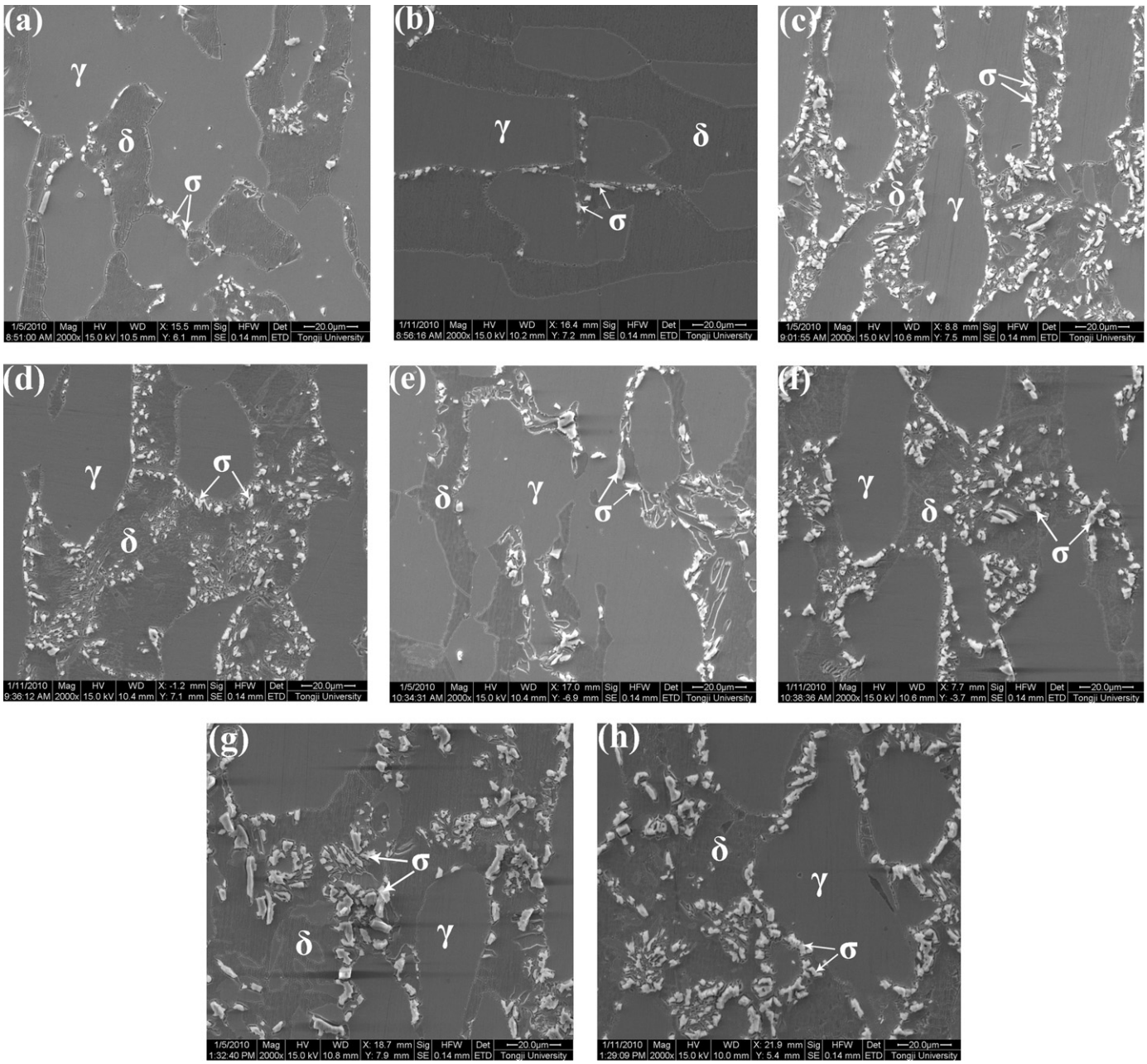

Fig. 2. SEM micrographs of the specimens: aged at 750 °C for 60 min after solution treatment at (a) 1060 °C and (b) 1230 °C; aged at 750 °C for 80 min after solution treatment at (c) 1060 °C and (d) 1230 °C; aged at 850 °C for 60 min after solution treatment at (e) 1060 °C and (f) 1230 °C; aged at 850 °C for 80 min after solution treatment at (g) 1060 °C and (h) 1230 °C.

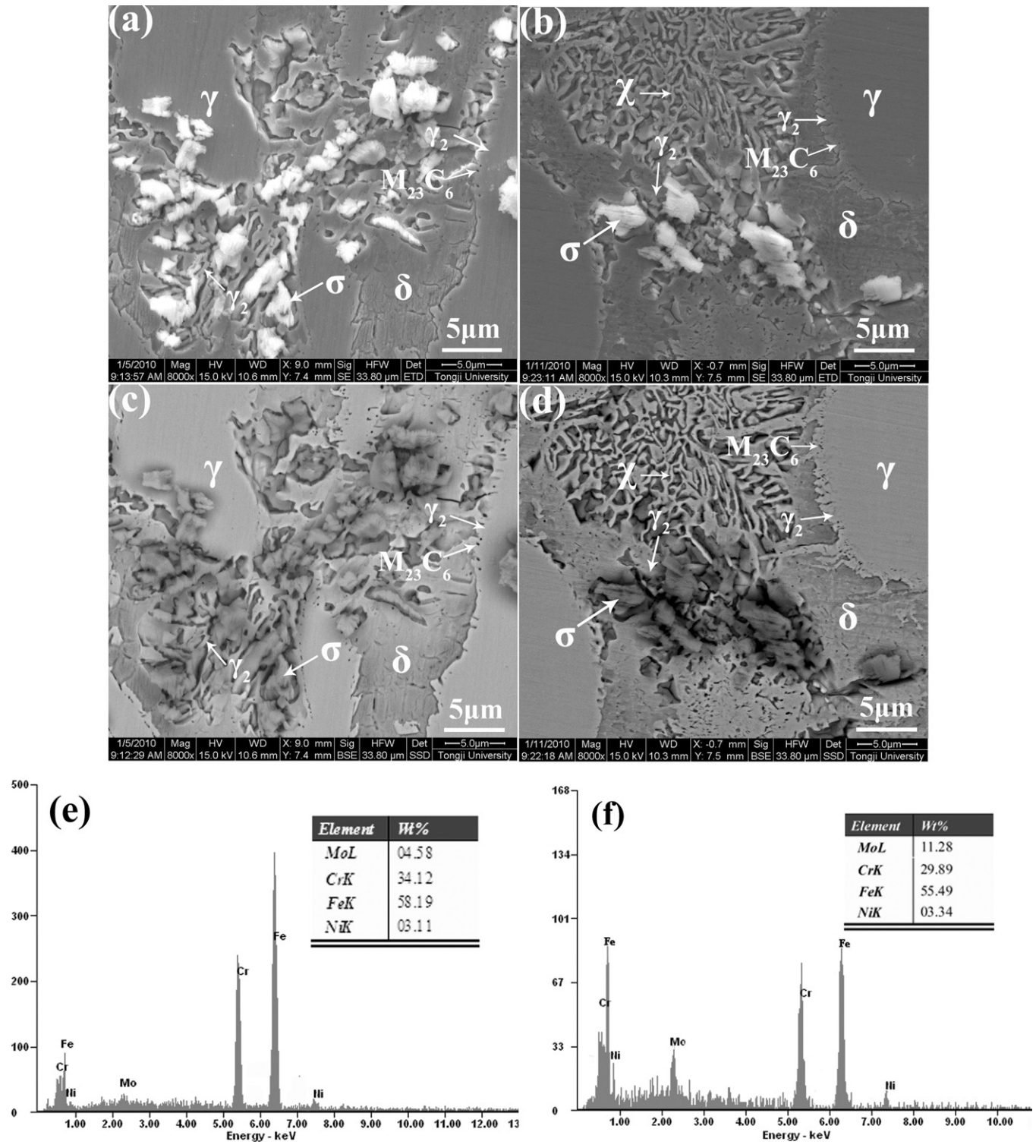

Fig. 3. Secondary electron images of the specimens aged at 750 °C for 80 min after solution treatment at (a) 1060 °C and (b) 1230 °C; corresponding BSE images of the specimens aged at 750 °C for 80 min after solution treatment at (c) 1060 °C and (d) 1230 °C; (e) EDS spectrum of σ-phase corresponding to (b); (f) EDS spectrum of χ-phase corresponding to (b).

Fig. 3 shows the secondary electron (SE) and back-scattered electron (BS) images of SEM obtained from the samples aged at 750 °C for 80 min after STT at 1060 °C (Fig. 3a and c) and 1230 °C (Fig. 3b and d), respectively. These micrographs were obtained from triple junction region of the samples, which possessed the most δ/γ and δ/δ interfaces in DSS, thus favoring the formation of σ-phases. And the σ-phase is closely associated with the δ/γ interface of duplex structure, often leading to a typical eutectoid structure of σ and γ_2 in the matrix of δ-ferrite grains. In the SE image of Fig. 3a and b, the region of δ-ferrite with lower level indicates that δ-ferrite grains are more sensitive to the electrolytical etching than γ grains. In the BS image of Fig. 3c, σ-particles precipitated at δ/γ and δ/δ interfaces and within δ-ferrite appearing as the darker area, and the dark contrast shows the σ-phase contains more elements with low atomic number due to chromium-richness. By contrast, fewer σ particles preferentially formed at the triple junction inter-

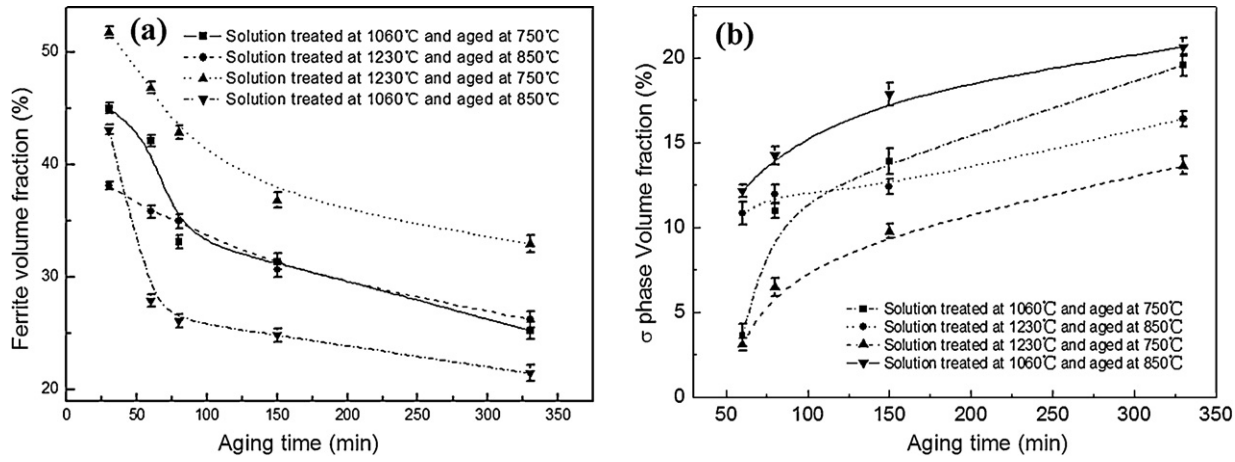

Fig. 4. Variation in the volume fraction of ferrite and σ-phase in 25% Cr DSS plotted as a function of ageing time after solution treatment at 1060 °C and 1230 °C.

faces (Fig. 3d). In addition, the initial decomposition of δ-ferrite occurred within δ-ferrite grains, indicating the Mo-rich χ-phase prior to σ-phase formed due to low interfacial energy of highly coherent χ/δ interface with a characteristic cubic-to-cubic orientation relationship [18]. Therefore, in Fig. 3b and d, it was observed that χ-phase formed at the initial stage of the decomposition of δ ferrite. The EDS results of both σ-phase and χ-phase corresponding to Fig. 3b are shown in Fig. 3e and f, respectively. The composition of χ-phase is $Fe_{36}Cr_{12}Mo_{10}$, which is of cubic structure and rich in Mo [19], whereas σ-phase is a kind of intermetallic compound rich in Cr and Mo. The content of Mo is higher than σ-phase, and the content of Cr is lower than σ-phase, which was proved by these EDS results. $M_{23}C_6$ was likely to precipitate in the γ/δ interface in the form of a string of carbide particles outlining the γ/γ_2 inter-phase boundaries. The growth of carbides along the δ/γ interface took place according to the transformation reaction $\delta \rightarrow M_{23}C_6 + \gamma_2$. Consequently, the higher STT delayed the process of σ-phase precipitation in the initial stage of high temperature ageing treatment.

3.2. Quantitative metallographic measurement of δ-ferrite phase and σ-phase

The volume fraction of δ-ferrite and σ-phase as a function of ageing time was plotted and shown in Fig. 4. Overall, the decomposition rate of δ-ferrite was fast within the initial ageing of 80 min, then got slower (Fig. 4a), whereas the amount of σ-phase increased corresponding to the decomposition of δ-ferrite (Fig. 4b). When the

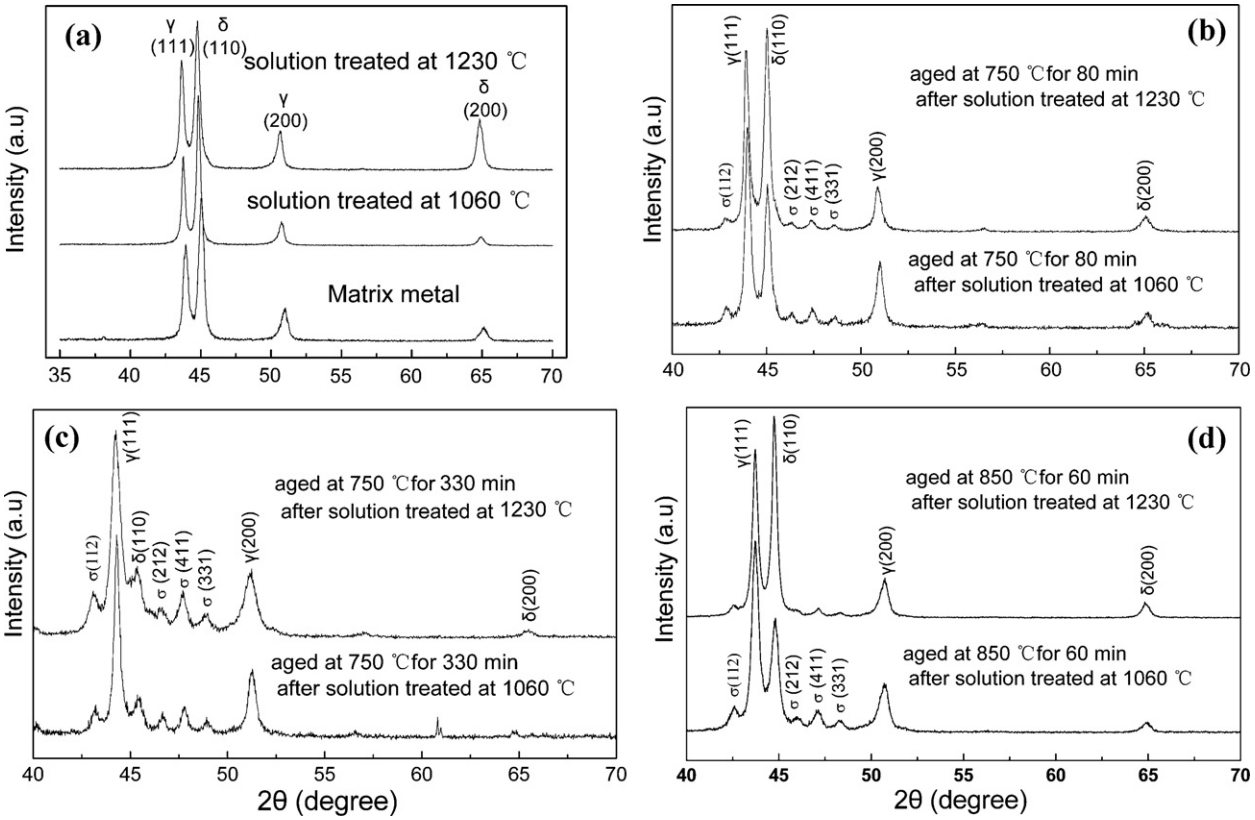

Fig. 5. XRD patterns of 25% Cr DSS subjected to solution treatment at 1060 °C and 1230 °C and then subjected to ageing time at 750 °C and 850 °C, respectively.

Table 2
The composition (wt.%) of austenite (γ), deta-ferrite (δ), sigma (σ) and surrounding sigma.

Elements	γ_a	δ_a	σ_a	Surrounding σ_a	γ_b	δ_b	σ_b	Surrounding σ_b
Ni	8.59 ± 0.1	4.28 ± 0.1	5.67 ± 0.1	16.28 ± 0.2	7.61 ± 0.1	6.12 ± 0.1	5.36 ± 0.1	18.52 ± 0.2
Cr	24.23 ± 0.2	28.32 ± 0.2	34.96 ± 0.3	10.24 ± 0.2	24.68 ± 0.2	26.82 ± 0.2	34.35 ± 0.3	11.98 ± 0.2
Mn	0.52 ± 0.1	0.47 ± 0.1	0.16 ± 0.05	0.46 ± 0.1	0.47 ± 0.1	0.59 ± 0.1	0.11 ± 0.05	0.48 ± 0.1
Mo	2.3 ± 0.1	3.76 ± 0.1	4.17 ± 0.1	2.23 ± 0.1	2.44 ± 0.1	3.56 ± 0.1	3.98 ± 0.1	2.78 ± 0.1
Fe	Bal.	Bal.	Bal.	Bal.	Bal.	Bal.	Bal.	Bal.

[a] Aged at 750 °C for 60 min after solution treated at 1060 °C.
[b] Aged at 750 °C for 60 min after solution treated at 1230 °C.

ageing time at 750 °C ranging from 60 min to 330 min, it can be seen from Fig. 4b that the STT at 1230 °C led to less volume fraction of σ-phase precipitation than 1060 °C. Moreover, in the early stage of ageing at 850 °C for 60 min, the retardation of σ-phase precipitation was not effective, which was attributed to higher diffusion rate of σ-phase forming element (Cr) in the δ-ferrite phase with higher ageing temperature. However, when the time of isothermal treatment was prolonged, less volume fraction of σ-phase precipitation occurred by increasing STT from 1060 °C to 1230 °C. Therefore, it is effective to delay the σ-phase formation ageing at 750 °C and 850 °C by means of higher prior-STT according to results of Fig. 2 and Fig. 4. Such phenomena are mainly related to the initial chromium content and the amount of δ/γ interfaces. Elevating STT can increase the amount of δ-ferrite [12], leading to less chromium and more nickel within δ-ferrite phase, and a lower concentration of chromium increases the time for $\delta \rightarrow \gamma_2 + \sigma$ transformation. We know that σ-phase forms more easily in the high-energy regions such as grain boundaries and interfaces. The δ/γ interfaces which contributed to preferential precipitation sites for σ-phase decreased by $\gamma \rightarrow \delta$ transformation, which was also proved by XRD results. Consequently, the higher prior-STT caused less amount of σ-phase precipitation during high temperature ageing, which is corresponding to the curvilinear trend as shown in Fig. 4b.

3.3. XRD and electron EDX analysis for different phases

The major X-ray diffractions from δ-ferrite and austenite and the minor diffractions from σ-phase can be identified in Fig. 5. The spectra for matrix metal and samples with solution treated at 1060 °C and 1230 °C respectively are presented in Fig. 5a. It can be seen that the major diffraction peaks of the δ-ferrite and austenite increased by enhancing STT from 1060 °C to 1230 °C, due to the strengthened solution effect of the δ-forming elements (Cr, Mo) and γ-forming elements (Ni, N). Furthermore, it was also observed that the intensity of the δ (1 1 0) and δ (2 0 0) peaks increased distinctly with higher STT, indicating that $\gamma \rightarrow \delta$ transformation occurred. Therefore, higher STT can cause lager δ-ferrite grain size and fewer potential nucleation sites for σ-phase formation during ageing [20]. With further ageing at 750 °C for 80 min (Fig. 5b), the σ-phase peaks appeared weaker at its corresponding peak position by increasing STT from 1060 °C to 1230 °C. Meanwhile, when the specimens were aged at 850 °C for 60 min, the intensity of the four σ-phase peaks appeared weaker with higher STT, which was corresponding to the reduction in the δ (1 1 0) peak as a result of $\delta \rightarrow \sigma + \gamma_2$ transformation (Fig. 5d). In the case of longer ageing treatment at 750 °C for 330 min, the intensity of δ (1 1 0) peak was much weaker, which exhibited that the decomposition of δ-ferrite finished well. By contrast, the intensity of σ-phase appeared stronger as shown in Fig. 5c, and the intensity of δ (1 1 0) became slight stronger due to higher STT. As a result, it is also proved that the σ-phase precipitation was suppressed due to higher STT (1260 °C) at the initial ageing, which was corresponding to the microstructure evolution results in Fig. 2.

The EDS results for the samples with prior-STT at 1060 °C and 1230 °C and ageing treatment at 750 °C for 60 min are summarised in Table 2. The results showed that chromium partitioned more to δ-ferrite, whereas nickel partitioned more to γ-austenite. In addition, σ-phase was partitioned in high Cr and Mo, and the surrounding region of σ-phase was low in Cr and high in Ni. It is well established that the growth of σ-phase particles during ageing develops by absorbing Cr and Mo atoms in the neighboring areas, leading to the Cr-depleted region around it. Consequently, in the early stage of ageing treatment (Table 2), the content of major elements (Cr and Mo) in δ-ferrite decreased by increasing STT from 1060 °C to 1230 °C, thus delaying the σ-phase precipitation due to decreased precipitation kinetics [10].

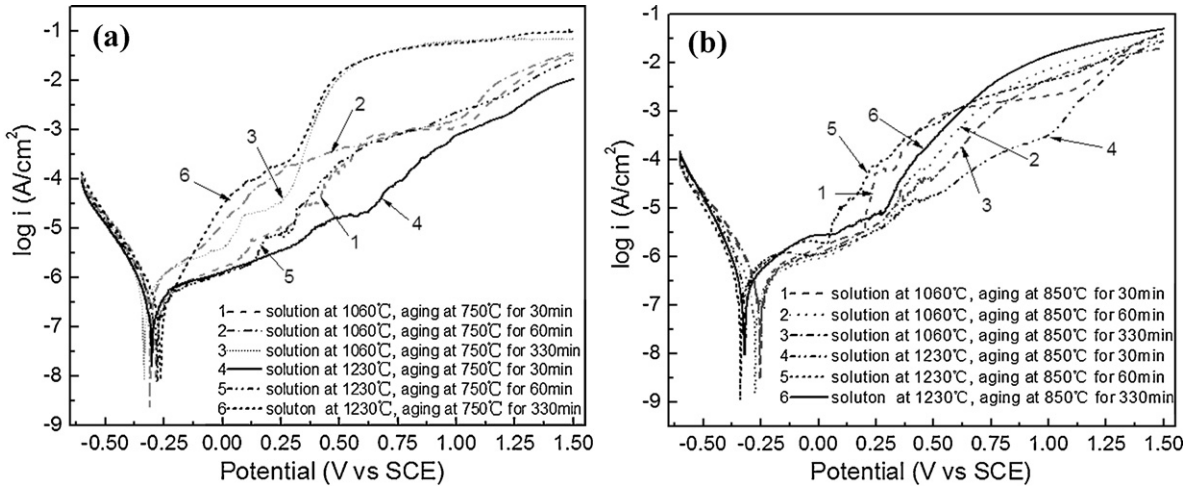

Fig. 6. Potentiodynamic polarization curves for 25% Cr DSS in 3.5 wt.% NaCl with potential scan rate at 1.5 mV/s aged at (a) 750 °C and (b) 850 °C after solution treatment at 1060 °C and 1230 °C. Curves 1, 2 and 3: solution treated at 1060 °C and curves 4, 5, 6: solution treated at 1230 °C.

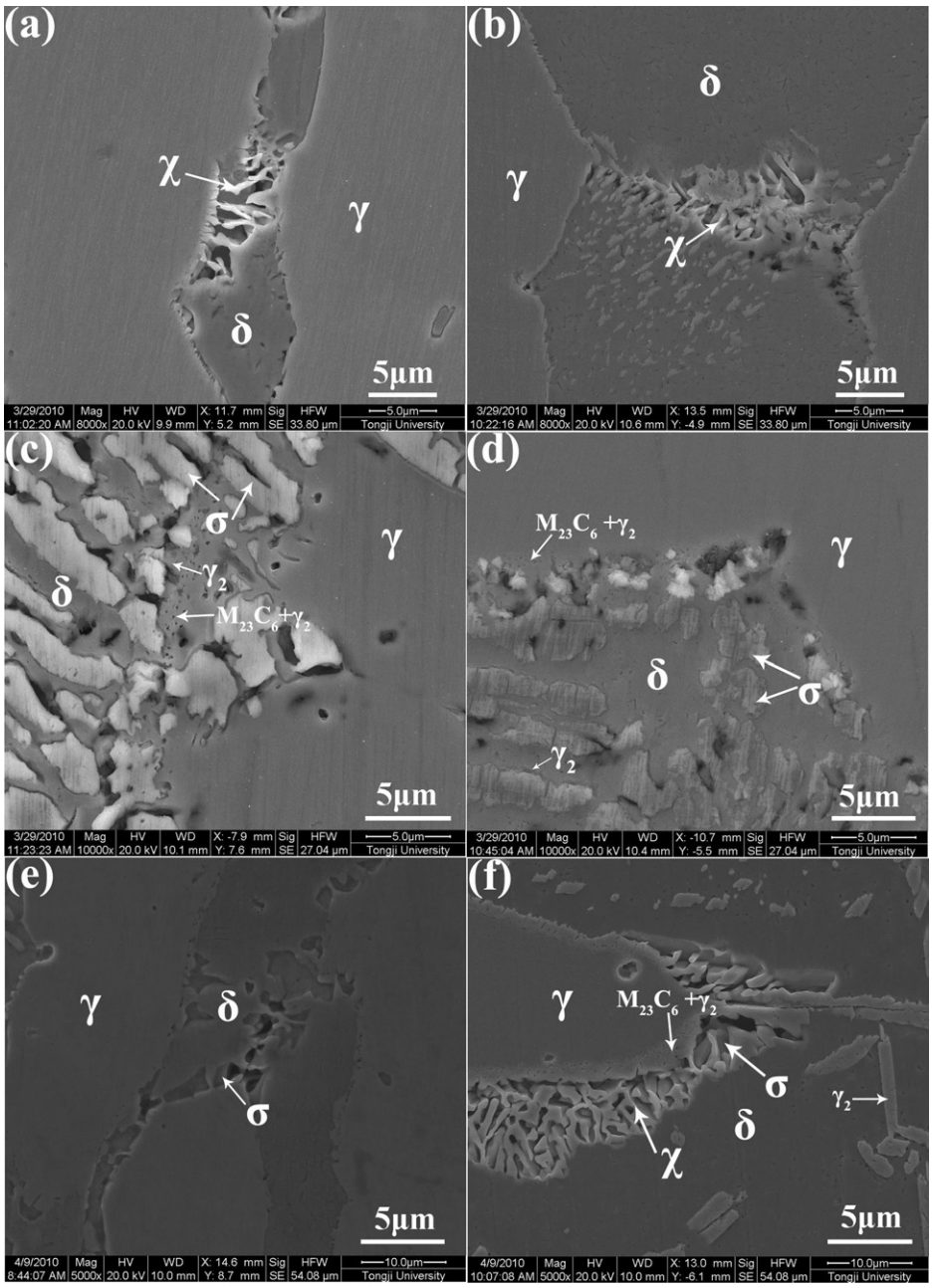

Fig. 7. The etched surface morphology of the specimens which were subjected to potentiodynamic polarization tests in 3.5% wt.% NaCl with potential scan rate 1.5 mV/s. The specimens aged at 750 °C for 30 min after solution treatment at (a) 1060 °C and (b) 1230 °C for 30 min; the specimens aged at 750 °C for 330 min after solution treatment at (c) 1060 °C and (d) 1230 °C for 30 min; the specimens aged at 850 °C for 30 min after solution treatment at (e) 1060 °C and (f) 1230 °C.

3.4. Potentiodynamic polarization

The influence of prior-STT on the corrosion resistance of the tested specimens was evaluated by the use of potentiodynamic polarization measurement. Fig. 6 shows the typical polarization curves which are close to the average polarization behavior under different solution and ageing treatment temperature. The anodic polarization curves provide useful information concerning the potential range over which a material is susceptible to pitting corrosion. The polarization curves marked as 1, 2 and 3 with STT at 1060 °C, and curves marked as 4,5 and 6 with STT at 1230 °C, were obtained from the specimens aged at 750 °C (Fig. 6a) and 850 °C (Fig. 6b) for 30 min, 60 min, 330 min, respectively. It was observed that the corrosion potential (E_{corr}) under different polarization curves varies slight, with the value of which is around −300 mV SCE. As the specimen was aged at 750 °C for 30 min after STT at 1230 °C, the corresponding curve 4 in Fig. 6a showed passive state at low potentials, then became transpassive above 1000 mV SCE, exhibiting the lowest corrosion rate. It was noted that the metastable pitting current density peak was not clear and was across a range of low potentials below the critical pitting temperature (CPT) [21]. Hence, there were small current oscillations between 150 mV to 700 mV in curves 1 and 5 in Fig. 6a, indicating that the metastable pitting may be initiated around this range and then led to stable pitting growth. On the other hand, there was an initial rapid increase in current density near the open circuit potential and a steady rise thereafter in curve 2 in Fig. 6a. By contrast, the curve 5 with higher STT (1230 °C) exhibits lower corrosion rate, which was

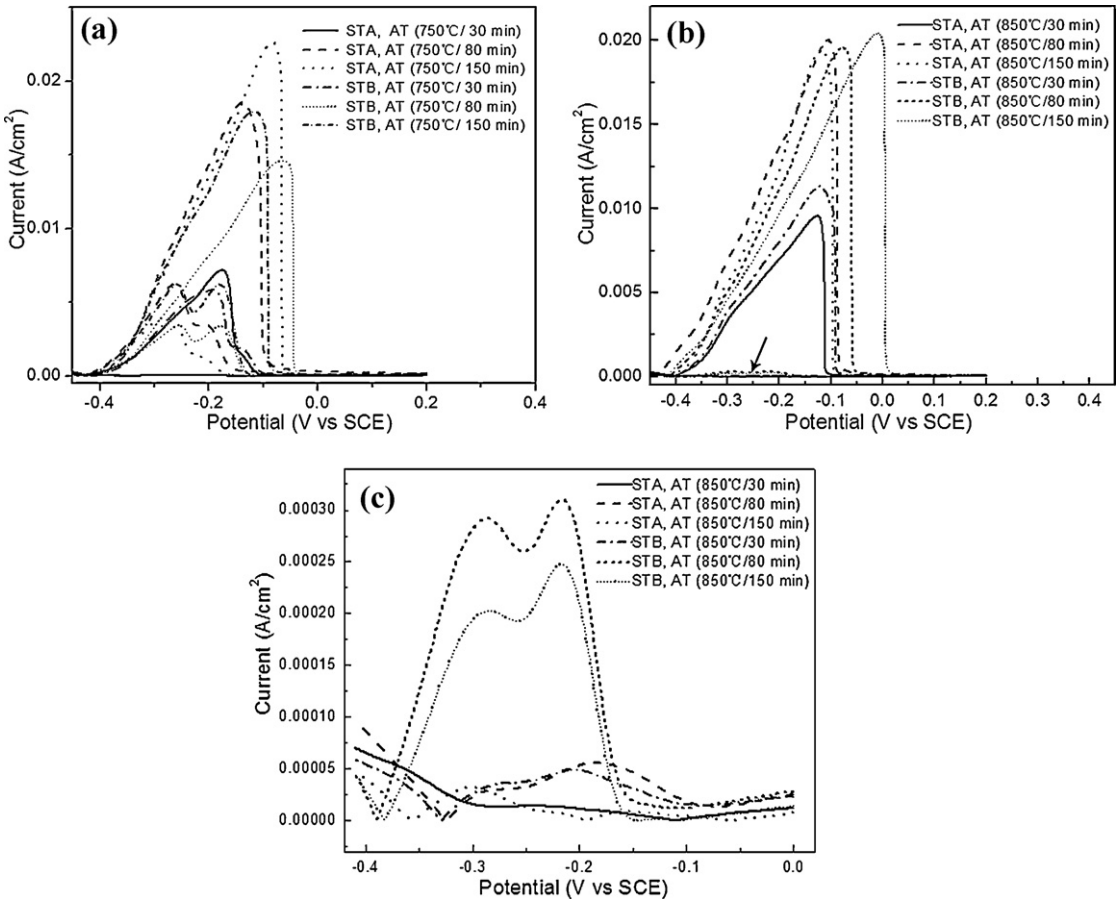

Fig. 8. DL-ERP curves plotted for DSS: (a) aged at 750 °C after solution treatment at 1230 °C and 1060 °C, respectively; (b) aged at 850 °C after solution treatment at 1230 °C and 1060 °C, respectively; (c) enlarged graph as indicated by arrow in (b).

attributed to retardation of σ-phase precipitation. Moreover, with longer ageing treatment at 750 °C up to 330 min, the curves 3 and 6 in Fig. 6a showed stable pitting transition at 250 mV SCE because more σ-phase formation lowered the CPT. As the ageing temperature increased to 850 °C (Fig. 6b), it was observed that small current oscillations occurred between 250 mV and 510 mV SCE, where the metastable pitting may be initiated. In addition, the current density increased steadily as the potential was shifted to more noble value after metastable events with curves 1, 3, 5 and 6, presenting better passivation behavior at low potentials. However, there was no abrupt current transition observed even in curves 3, 6 with ageing time up to 330 min, where more σ-phase precipitation occurred. It could be interpreted by that higher ageing temperatures (850 °C) favored the diffusion of Cr atoms from δ-ferrite matrix. Hence, the Cr-depleted region around σ precipitates could thus be recovered to some extent compared with ageing treatment at 750 °C.

3.5. Corrosion morphology after potentiodynamic measurements

Fig. 7 presents SE images of etched surface for specimens after potentiodynamic measurements. It is noted that χ-phase occurs preferentially at δ/γ interfaces and at δ/δ grain boundaries, and precipitates at δ/δ grain boundaries prior to the σ-phase precipitation [22]. Therefore, in the initial stage of ageing treatment at 750 °C for 30 min after different solution treatment, as shown in Fig. 7a and b, χ-phase formed at γ/δ and δ/δ interfaces. It was observed that a few visible metastable black pits were initiated at γ/δ interfaces and near the χ-phase, appearing smaller by increasing STT from 1060 °C (Fig. 7a) to 1230 °C (Fig. 7b). When the specimen was subjected to a longer ageing treatment at 750 °C for 330 min after STT at 1060 °C, as presented in Fig. 7c, the stable pitting with black region took place within the δ-ferrite matrix, and was mainly located in active regions around coarse σ precipitates and at σ/δ and $M_{23}C_6$/δ interfaces. This case may be due to the presence of Cr- and Mo-depleted zones of δ-phase in the vicinity of σ precipitates. Moreover, γ_2-phase formed at σ/δ and at $M_{23}C_6$/δ interfaces by eutectoid reactions of $\delta \rightarrow M_{23}C_6 + \gamma_2$ and $\delta \rightarrow \sigma + \gamma_2$ as shown in Fig. 7, which has been reported to provide preferential sites as well for pitting attack because of lower Cr concentration than in most of γ-phase [23]. Park et al. [24] suggested that the region of $\delta + \gamma_2$ was sensitive to active dissolution by using the droplet cell. By contrast, less amount of smaller pits formed around coarse σ precipitates and at σ/δ interfaces by increasing STT from 1060 °C (Fig. 7c) to 1230 °C (Fig. 7d), which can be accounted for by that higher STT led to less amount of smaller σ-phase precipitation, thus reducing Cr-depleted regions within δ-ferrite phase and at grain boundary interfaces. Fig. 7e and f showed the etched surface morphology of the specimens aged at 850 °C for 30 min after STT at 1060 °C and 1230 °C, respectively. It can be found that the metastable pits preferentially formed at the triple junction interfaces. More untransformed χ-phase appeared within triple junction interfaces and an amount of γ_2 was dispersed in δ-ferrite with higher STT (Fig. 7f), corresponding to lower corrosion rate under curve 4 in Fig. 6b. In addition, the selective corrosion/attack of ferrite phase in this duplex stainless steel was likely to occur after pitting attack. As we know, such selective attack is a type of corrosion in alloys, when in suitable conditions a component of the alloys is preferentially leached from the material. The less noble metal is removed from the alloy by microscopic-scale galvanic corrosion mechanism. A great number of σ precipitates causing surrounding

Table 3
Results of the double-loop electrochemical potentiokinetic reactivation (DL-EPR) test.

Sample identification	Heat treatment conditions	I_a, 10^{-2} (A/cm^{-2})	I_r, 10^{-5} (A/cm^{-2})	$R_a = I_r/I_a$ (%)
1l	STA[a], AT[c] (750 °C/30 min)	0.719	6.84	0.95
l2	STA, AT (750 °C/80 min)	1.868	623	12.3
l3	STA, AT (750 °C/150 min)	2.263	406	17.9
l4	STB[b], AT (750 °C/30 min)	0.585	6.87	1.17
l5	STB, AT (750 °C/80 min)	1.461	340	23.3
l6	STB, AT (750 °C/150 min)	1.794	619	34.5
h1	STA, AT (850 °C/30 min)	0.957	1.213	0.127
h2	STA, AT (850 °C/80 min)	2	5.535	0.277
h3	STA, AT (850 °C/150 min)	1.94	3.168	0.163
h4	STB, AT (850 °C/30 min)	1.13	4.898	0.433
h5	STB, AT (850 °C/80 min)	1.96	30.95	1.58
h6	STB, AT (850 °C/150 min)	2.05	24.79	1.21

[a] STA, solution treatment at 1230 °C for 30 min.
[b] STB, solution treatment at 1060 °C for 30 min.
[c] AT, ageing treatment.

area lack of Cr especially in the longer ageing of 330 min. Hence, the Cr-depleted area corresponded to broken passive film was easily attacked by chloride ion and formed pits during the process of potentiodynamic scanning in the NaCl solution. Selective corrosion can easily take place on the basis of these pits. Therefore, the presence of many pits led to selective corrosion in the Cr-depleted area surrounding σ precipitates.

3.6. Evaluation of intergranular corrosion by DL-ERP tests

As stated above, the loss of intergranular resistance due to Cr-depleted regions was evaluated by the ratio as $R_a = I_r/I_a$, where I_a and I_r are the current peak density in the anodic scan and reversed scan, respectively. Fig. 8 shows typical DL-ERP curves obtained from specimens aged at 750 °C and 850 °C after STT at 1060 °C and 1230 °C, respectively. All the specimens presented a wide passivity range approximately from 0 to 200 mV SCE, with anodic current density close to 3×10^{-5} A cm^{-2}, and I_a increased proportionally with prolonged ageing time. This peak may be attributed to the active dissolution of alloying elements. In addition, Table 3 shows the list of I_a, I_r, and I_r/I_a determined by DL-EPR test results. The sample identifications labeled in Fig. 8 is corresponding to that shown in Table 3. In the case of initial ageing at 750 °C for 30 min (Fig. 8a), the maximum current density in the anodic scan is 7.19×10^{-3} A cm^{-2} and 5.85×10^{-3} A cm^{-3} with STT at 1230 °C and 1060 °C respectively, which mounted rapidly with ageing at 750 °C up to 80 min and 150 min. However, the magnitude of the reactivation peak currents varied significantly with the degree of sensitization, which was initially very small, of approximately 6.84×10^{-5} A cm^{-2} and 6.87×10^{-5} A cm^{-2} with the samples aged at 750 °C for 30 min after STT at 1230 °C and 1060 °C respectively, then rose rapidly with ageing time up to 80 min and 150 min. Moreover, Fig. 8b presents the DL-ERP curves plotted for specimens aged at 850 °C after STT at 1230 °C and 1060 °C, respectively. As can be seen, the difference of the peaks in the anodic scan appeared slightly with different STT, but higher STT led to weaker reactivation current peaks as shown in the enlarged photograph (Fig. 8c). The degree of sensitization (R_a) of specimens with ageing at 750 °C and 850 °C after STT at 1060 °C and 1230 °C is shown in Table 3. With STT at 1060 °C, the value of R_a increased rapidly from 1.17% to 34.5% with ageing treatment at 750 °C from 30 min to 330 min. In the low-carbon DSS, where $Cr_{23}C_6$ is relatively scarce, more precipitates of σ-phases can cause Cr-depleted zones around the grain boundary [10], leading to a decrease in resistance to IGC in severely sensitised specimen. However, when the STT mounted to 1230 °C, the value of R_a became smaller with ageing treatment at 750 °C. Consequently, increasing STT can cause smaller localised Cr- and Mo-depleted areas around the σ-phase. And the value of R_a dropped because of less amount of σ-phase formed at γ/δ grain boundaries, contributing to better resistance to IGC. On the other hand, when the DSS was subjected to ageing treatment at 850 °C ranging from 30 min to 330 min, the value of R_a dropped much more as shown in Table 3. This may be interpreted by that Cr-depleted zones at grain boundary gained recovered as a result of the enhanced role of Cr diffusion at higher ageing temperature. In addition, it is observed that the value of R_a was lowered with ageing at 850 °C with elevated STT.

4. Conclusions

By studying the effect of the prior-STT on the microstructure and corrosion behavior in 25% Cr DSS after ageing at 750 °C and 850 °C, the following results were obtained:

(1) In the early stage of ageing at 750 °C and 850 °C for 60 min, the precipitation rate of σ-phase was fast, then got slower with ageing time up to 330 min. The σ-phase formation was effectively suppressed by increasing STT from 1060 °C to 1230 °C especially with ageing at 750 °C. This was attributed to the reduction of δ/γ interfaces and the decrease of σ-phase forming element (Cr) concentration.
(2) With ageing treatment at 750 °C up to 150 min, the retardation of σ-phase precipitation lowered the corrosion rate of the specimen due to higher STT. In addition, the transition from metastable to stable pitting occurred with a longer ageing treatment at 750 °C for 330 min. The specimen ageing at 850 °C showed better passivation behavior at low potentials due to the recovering effect of Cr atoms diffusion to the Cr-depleted region.
(3) A few of smaller metastable pits initiated near χ-phase and at γ/δ interfaces in the initial stage of ageing at 750 °C due to higher STT. With a longer ageing treatment at 750 °C for 330 min, less amount of smaller pits appeared in the regions around coarse σ precipitates and at σ/δ interfaces due to higher STT at 1230 °C.
(4) DL-ERP tests indicate that more precipitation of σ-phase can lead to specimens more prone to IGC with prolonged ageing time. Higher STT contribute to the increase in resistance to IGC with ageing at 750 °C and 850 °C. There was an indication of recovering and a decreased degree of sensitization value for specimens aged at 850 °C.

References

[1] M.B. Cortie, E.M.L.E.M. Jackson, Metall. Mater. Trans. A. 28A (1996) 1997–2477.
[2] T. Maki, T. Furuhara, K. Tsuzaki, ISIJ Int. 41 (2001) 571–579.
[3] V. Muthupandi, P.B. Srinivasan, S.K. Seshadri, S. Sundaresan, Mater. Sci. Eng. A A358 (2003) 9–16.

[4] W. Horvarth, W. Prantl, H.P. Stuwe, E. Werner, Mater. Charact. 34 (1995) 277–285.
[5] C.S. Huang, C.C. Shih, Mater. Sci. Eng. A A402 (2005) 66–75.
[6] O. Smuk, Y.U. Jagodzinski, O. Tarasenko, S. Smuk, H. Hanninen, Scr. Mater. 40 (1999) 321–326.
[7] M. Pohl, O. Storz, T. Glogowski, Mater. Charact. 58 (2007) 65–71.
[8] T.H. Chen, K.L. Weng, J.R. Yang, Mater. Sci. Eng. A 338 (2002) 270–271.
[9] E. Johnson, Y.J. Kim, L.S. Chumbley, B. Gleeson, Scr. Mater. 50 (2004) 1351–354.
[10] K.N. Adhe, V. Kain, K. Madangopal, H.S. Gadiyar, J. Mater. Eng. Perform. 5 (1996) 500–506.
[11] N. Lopez, M. Cid, M. Puiggali, I. Azkarate, A. Pelayo, Mater. Sci. Eng. A 229 (1997) 123–128.
[12] J.K.L. Lai, K.W. Wong, D.J. Li, Mater. Sci. Eng. A 203 (1995) 356–364.
[13] R. Badji, M. Bouabdallah, B. Bacroix, C. Kahloun, K. Bettahar, N. Kherrouba, Mater. Sci. Eng. A 496 (2008) 447–454.
[14] T.H. Chen, J.R. Yang, Mater. Sci. Eng. A 311 (2001) 28–41.
[15] J.-O. Nilsson, P. Kangas, T. Karlsson, A. Wilson, Metall. Trans. A 31A (2000) 35–45.
[16] ASTME 562 standard practice for Determining Volume Fraction by Systematic Manual Point Count.
[17] R. Chaves, I. Costa, H.G. Melo, S. Wolynec, Electrochim. Acta 51 (2006) 1842–1846.
[18] T.H. Chen, K.L. Weng, J.R. Yang, Mater. Sci. Eng. A 338 (2002) 259–270.
[19] J.S. Kasper, Acta Metall. 2 (1954) 456–461.
[20] K.M. Lee, H.S. Cho, D.C. Choi, J. Alloys Compd. 285 (1999) 156–161.
[21] L.F. Garfias-Mesias, J.M. Sykes, Corros. Sci. 41 (1999) 959–987.
[22] D.M. Escribaa, E. Materna-Morris, R.L. Plaut, A.F. Padilha, Mater. Charact. 60 (2009) 1214–1219.
[23] C.H. Shek, C. Dong, J.K.L. Lai, K.W. Wong, Metall. Trans. A 31A (2000)15.
[24] C.J. Park, H.S. Kwon, M.M. Lohrengel, Mater. Sci. Eng. A 372 (2004) 180–185.